PHYSICAL REVIEW D **94,** 094032 (2016)

Tetraquark bound states and resonances in a unitary microscopic quark model: A case study of bound states of two light quarks and two heavy antiquarks

P. Bicudo[*] and M. Cardoso[†]

CFTP, Departamento de Física, Instituto Superior Técnico, Universidade de Lisboa, Avenida Rovisco Pais, 1049-001 Lisboa, Portugal

(Received 16 September 2015; revised manuscript received 14 October 2016; published 23 November 2016)

We address $qq\bar{Q}\bar{Q}$ exotic tetraquark bound states and resonances with a fully unitarized and microscopic quark model. We propose a triple string flip-flop potential, inspired by lattice QCD tetraquark static potentials and flux tubes, combining meson-meson and double Y potentials. Our model includes the color excited potential, but neglects the spin-tensor potentials, as well as all the other relativistic effects. To search for bound states and resonances, we first solve the two-body mesonic problem. Then we develop fully unitary techniques to address the four-body tetraquark problem. We fold the four-body Schrödinger equation with the mesonic wave functions, transforming it into a two-body meson-meson problem with nonlocal potentials. We find bound states for some quark masses, including the one reported in lattice QCD. Moreover, we also find resonances and calculate their masses and widths, by computing the T matrix and finding its pole positions in the complex energy plane, for some quantum numbers. However, a detailed analysis of the quantum numbers where binding exists shows a discrepancy with recent lattice QCD results for the $ll\bar{b}\bar{b}$ tetraquark bound states. We conclude that the string flip-flop models need further improvement.

DOI: 10.1103/PhysRevD.94.094032

I. INTRODUCTION

A long-standing problem of QCD is the search for localized exotic states [1] and the corresponding decay to the hadron-hadron continuum. There is no QCD theorem preventing the existence of exotic hadrons, say two-gluon glueballs, hybrids, tetraquarks, pentaquarks, three-gluon glueballs, hexaquarks, and the scientific community continues to search for clear exotic candidates. However, this problem turned out to be much harder than expected.

In this work, we develop fully unitary techniques to solve some of the theoretical problems of multiquarks, and we predict multiquark bound states and resonances. We continue a previous unitary study of tetraquarks—here understood as any $q_1q_2\bar{q}_3\bar{q}_4$ bound state or resonance, independently of its color state—with a simplified two-variable toy model [2], now fully solving the tetraquark problem, of the Schrödinger equation for two quarks and two antiquarks, while still employing a completely nonrelativistic framework. We specialize in systems that are clearly exotic tetraquarks, which cannot have a significant mesonic quark-antiquark component, i.e., where the quantum numbers or the S matrix pole and decay amplitudes clearly show it is a tetraquark.

In particular, as a benchmark, we study in detail the light-light-antiheavy-antiheavy systems that are expected to produce tetraquarks. From basic principles of QCD, it is clear that a system with two light quarks and two heavy antiquarks, for instance with flavor $ud\bar{b}\bar{b}$, should form a bound state if the antiquarks are heavy enough [3–13]. To understand why binding should occur, it is convenient to use the Born-Oppenheimer [14] perspective, where the wave function of the two heavy antiquarks is determined considering an effective potential integrating the light quark coordinates. At very short $\bar{b}\bar{b}$ separations r, the $\bar{b}$ quarks interact with a perturbative one-gluon-exchange Coulomb potential, while at large separations the light quarks totally screen the interaction and the four quarks form two rather weakly interacting B mesons as discussed in Ref. [15]. Thus a screened Coulomb potential is expected. This potential clearly produces a bound state, providing the antiquarks $\bar{b}\bar{b}$ are heavy enough.

We leave a comparison of our work with previous tetraquark studies in the literature for Sec. II. We discuss the searches for tetraquarks in experiments, in dynamical lattice QCD, in semidynamical lattice QCD with quantum mechanical techniques, and in quark models. In Sec. III we describe our triple string flip-flop potential, where our system is open to the continuum in the meson-meson directions and is confined in the diquark-diantiquark direction. Our string flip-flop potential also includes the first color excitation. In Sec. IV, we address the meson-meson scattering problem, occurring when we solve the Schrödinger equation. We detail our numerical techniques, utilized to solve both our bound state and scattering problems. In Sec. V we show our results with the state of the art triple

[*]bicudo@tecnico.ulisboa.pt
[†]mjdcc@cftp.ist.utl.pt

string flip-flop potential, exhibiting tetraquark bound states, and resonances. For the resonances, with our fully unitarized computation, we calculate the pole position and thus find their decay widths. We also consider, to compare with our full computation, simplified potentials. In Sec. VI we compare our results to the existing lattice QCD results for the light-light-antiheavy-antiheavy system and conclude. We find excessive binding, concluding that the flip-fop potentials need further improvement. Nevertheless, our technique can be applied to other potentials that may be developed in the future. Moreover, in Appendix A, as a benchmark calculation, we compare the results of our variational basis for the binding energy with the one of Ref. [13].

II. COMPARING OTHER STUDIES OF TETRAQUARKS WITH THE PRESENT WORK

A. The experimental search for tetraquarks

This is a very difficult problem experimentally, since exotic candidates are resonances immersed in the excited hadron spectra, and moreover, they usually decay to several hadrons.

For instance, the observation [16] of a $\pi_1(1600)$ resonance with exotic $J^{PC}=1^{-+}$ quantum numbers is consistent with an hybrid meson or a tetraquark. But it has not been confirmed yet, and similar π_1 candidates have been criticized in the past [17,18].

More related to our study of double-heavy tetraquarks, the charged $Z_c^{\pm}$ and $Z_b^{\pm}$ are cryptoexotic, but technically they can be regarded as essentially exotic tetraquarks if we neglect $c\bar{c}$ or $b\bar{b}$ annihilation. There are two $Z_b^{\pm}$ observed only by the BELLE Collaboration at KEK [19], slightly above the $B\,\bar{B}^*$ and $B^*\,\bar{B}^*$ thresholds, the $Z_b(10610)^+$ and $Z_b(10650)^+$. Their nature is possibly different from the two $Z_c(3940)^{\pm}$ and $Z_c(4430)^{\pm}$, where the masses are well above the DD threshold [20]. The $Z_c^{\pm}$ has been observed with very high significance and has received a series of experimental observations by the BELLE Collaboration [21,22], the Cleo-C Collaboration [23], the BESIII Collaboration [24–28], and the LHCb Collaboration [29]. This family is possibly related to the closed-charm pentaquark recently observed at LHCb [30]. Notice that, using very approximate resonant group method calculations, in 2008, we predicted [31] a partial decay width to $\pi J/\psi$ of the $Z_c(4430)^-$ consistent with the recently observed experimental value [29]. However, to establish a new resonance it is necessary to study with an accurate level of confidence all its properties, including its mass and width as determined by its S matrix pole and all relevant partial decay widths. Thus our option is to leave the detailed study of this complex family of double-heavy tetraquarks, with closed charm or closed bottom tetraquarks, for future studies.

We first want to address more constrained double-heavy tetraquarks with identical fermions, where the Pauli symmetry applies. It has already been predicted that double-charm hadrons can be produced experimentally [32,33].

B. The lattice QCD search for tetraquarks

1. Lattice QCD studies with dynamical and quenched quarks

In lattice QCD, the study of exotics is presently even harder than in the laboratory, since the techniques and computer facilities necessary to study resonances with many decay channels remain under development.

Thus lattice QCD started by searching for the expected bound state in light-light-antiheavy-antiheavy channels [34,35]. Using dynamical quarks, the only heavy quark presently accessible to lattice QCD simulations is the charm quark. No evidence for bound states in this family of tetraquarks, say for a $ud\bar{c}\bar{c}$, was found.

Lattice QCD also searched for evidence of a large tetraquark component in the closed charm, the $Z_c(3940)^-$ candidate [36,37]. The difficulty of the study of the Z_c^-, a resonance well above threshold, is due to its many two-meson coupled channels. The authors considered 22 two-meson channels, corresponding to lattice QCD interpolators $O^{M_1M_2}$. In addition, they considered 4 tetraquark channels, corresponding to diquark-antidiquark interpolators with flavor and color $[\bar{c}\bar{u}]_3\ [cd]_{\bar{3}}$. Evidence for the tetraquark resonance candidate was investigated in the full coupled correlator matrix of hadron operators.

Finally, after switching on and off the 4 tetraquarklike channels, the authors [36,37] found no significant deviation in the 13 lowest channels, which span the energy range from the lowest threshold to the $Z_c(3940)^-$ candidate. Thus, the authors concluded there is no robust evidence of a $Z_c^{\pm}$ tetraquark resonance.

However, the direct proof for, or against, a tetraquark resonance in lattice QCD would require the study of the S matrix. The technique to perform phase shift analysis in lattice QCD is still under development [38,39]. From the phase shift analysis, inasmuch as with experimental data, the poles of the S matrix can be extracted. But phase shift analysis of the tetraquark Z_c^+ has not yet been done with lattice QCD data. For absolute evidence, the different partial decay widths should be computed as well in lattice QCD.

In lattice QCD and with present computers, only resonances with a number of open decay channels of the order of unity have been studied with sufficient detail [40]. Recently the method of extracting the phase shifts from the spectrum of harmonic waves in a box started to be extended to inelastic (more than one open channel) coupled channels [41]. However, tetraquarks are excited resonances, decaying into many, ∼30, different channels for the last experimental Z_c^- candidates. This is unattainable by present computers and codes, but we expect lattice QCD to be on

the way to reach, in the future, the level of experimental data analysis.

2. Lattice QCD studies with two light quarks and two static antiquarks

The difficulties of using four dynamical quarks can be relaxed when one uses a hybrid approach with both numerical and quantum mechanics techniques.

Recently, the potentials between two mesons, each composed of a light quark and a static (or infinitely heavy) antiquark, have been computed in lattice QCD [42,43]. A static antiquark constitutes a good approximation to a spin-averaged $\bar{b}$ bottom antiquark. The potential between the two light-static mesons can then be used, with the Born-Oppenheimer approximation [14], as a $B-B$ potential, where the higher order $1/m_b$ terms including the spin-tensor terms are neglected. According to the quantum numbers of the two dynamical light quarks, either attraction or repulsion is found. The attraction/repulsion can be understood with the screening mechanism [15] leading to the screened Coulomb ansatz,

$$V(r) = -\frac{\alpha}{r}\exp\left(-\left(\frac{r}{d}\right)^p\right) + V_0. \tag{1}$$

Utilizing the potential of the channel with larger attraction, occurring in the isospin $= 0$ and spin $= 0$ quark-quark system, together with the Born-Oppenheimer approximation [14] to produce a Schrödinger equation for the heavy quarks, the possible bound states of the heavy antiquarks are then investigated with quantum mechanics techniques. Recently, this approach indeed found evidence for a tetraquark $ud\bar{b}\bar{b}$ bound state [15,44], while no bound states have been found for states where the heavy quarks are $\bar{c}\bar{b}$ or $\bar{c}\bar{c}$ (consistent with full lattice QCD computations [34,35]) or where the light quarks are $\bar{s}\bar{s}$ or $\bar{c}\bar{c}$ [45]. The $\bar{b}\bar{b}$ probability density in the only binding channel has also been computed in Ref. [15].

Important for the present study, the attraction and repulsion found in lattice QCD are consistent with the screening model:

(i) In some channels we find attraction, and in others we find repulsion.
(ii) As expected from the short range one-gluon exchange proportional to the Gell-Mann $\lambda^i \cdot \lambda^j$ Casimir operator, the $\bar{b}$ and $\bar{b}$ are attracted only if they are in a triplet 3, not a sextet 6.
(iii) Thus the light quarks qq must as well be in a color antitriplet $\bar{3}$.
(iv) Because of the Pauli principle this is indeed consistent with an s-wave, $I = 0$, and $S = 0$ diquark.

These results [45] for repulsion, attraction, or binding are very important for our study; in particular, our quark model results should comply with them.

C. Quark model approaches to exotic tetraquarks

A detailed theoretical understanding of the properties of exotic hadrons is important to support the experimental and lattice QCD searches of exotics. In our study we utilize solutions already adopted to address different theoretical problems of exotic hadrons.

1. On the early quark models

Already at the onset of QCD, the bag model predicted many tetraquarks [1]. However, as soon as lattice QCD was able to compute static quark potentials and color electromagnetic fields, it was realized that quark confinement was not baglike, but stringlike, due to color flux tubes.

Inspired by lattice QCD linear confining potentials, the relativized quark model potential was developed [46,47], after the authors fitted the spectra of all known hadrons in the 1980s. Notice that a correctly calibrated quark model needs many terms and many parameters, say of the order of ~20 parameters.

Nevertheless, the relativized quark model still lacks two crucial effects, leading up to 400 MeV deviations from its spectrum. Chiral symmetry breaking has since then been included in the Dyson-Schwinger approach [48,49], and coupled channels/unquenching that have also been included, for instance, in effective meson or baryon models [50,51].

2. Extra binding with four-body flux tube potentials

Moreover, since tetraquarks are always open to decays into a meson-meson pair, tetraquark resonances or bound states may exist only if a mechanism provides binding specific to tetraquarks. Here we explore a mechanism observed in lattice QCD static potentials: the confining four body potential [52,53], produced by double Y or butterfly shaped flux tubes or strings, observed in Ref. [54–56]. This mechanism is related to the Jaffe-Wilczek model [57–59], which proposed the tetraquark would form a diquark-antidiquark system.

We acknowledge other mechanisms may exist to support binding; however, they are quite complex to implement, and it is not clear, from lattice QCD, how they work quantitatively. For instance, attraction may also be due to quark-antiquark annihilation; however, this turned out to be insufficient to bind a proposed pentaquark [60,61]. Another mechanism is the hyperfine spin-dependent potential utilized in the original bag model [1]; however, the spin-tensor potentials have only been computed in lattice QCD for mesons [62]. For baryons they are model dependent, while for multiquarks the details of the spin-tensor potentials remain an open problem. Moreover, both quark-antiquark annihilation and the hyperfine potential are also important for chiral symmetry breaking. To avoid the complexity of quark-antiquark annihilation, spin-tensor quark-quark interactions, and chiral symmetry breaking, we specialize

in a family of tetraquarks where they can be neglected. Our tetraquark masses or poles should be seen as spin-averaged results.

Here we consider purely exotic tetraquarks only. In contradistinction to cryptoexotics, in pure exotics quark-antiquark annihilation does not occur directly. Cryptoexotic tetraquarks are also less clear in the sense they always have a mesonic component (as well as a multimeson component). They are never a pure exotic.

Thus we consider only tetraquarks with absolutely exotic flavor. Moreover, as a first study, we neglect chiral symmetry breaking effects. Nevertheless, we implement the unitarization in the tetraquark systems, since unquenching is unavoidable when studying resonances.

3. Solving the Van der Waals force problem with string flip-flop potentials

Clearly, tetraquarks are always coupled to meson-meson systems, and we must be able to address correctly the meson-meson interactions.

Notice confining two-body potentials with the SU(3) color Casimir invariant $\vec{\lambda}_i \cdot \vec{\lambda}_j$ suggested by the one-gluon-exchange potential, and possibly compatible with lattcie QCD, lead to a Van der Waals potential,

$$V_{\text{Van der Waals}} = \frac{V'(r)}{r} \times T, \tag{2}$$

where T is a polarization tensor. This would lead to an extremely large Van der Waals [63–68] force between mesons or baryons, which clearly is not observed experimentally. Thus two-body confinement dominance is ruled out for multiquark systems.

The string flip-flop potential for the meson-meson interaction was developed [57,69–72] to solve the problem of the Van der Waals forces produced by the two-body confining potentials.

Traditionally, the string flip-flop potential considers that the potential is the one minimizing the energy of the possible two different meson-meson configurations, say $M_{13}M_{24}$ or $M_{14}M_{23}$. This removes the intermeson potential, and thus solves the problem of the Van der Waals force.

Here we consider an upgrade the string flip-flop potential, including a third possible configuration [73], the tetraquark one, say $T_{12,34}$, where the four constituents are linked by a connected string [13,74]. We study whether the tetraquark attractive flux tube may induce further binding of tetraquarks.

The three configurations differ in the strings linking the quarks and antiquarks, and this is illustrated in Fig. 1. When the diquarks qq and $\bar{q}\bar{q}$ have small distances, the tetraquark configuration minimizes the string energy. When the quark-antiquark pairs $q\bar{q}$ and $q\bar{q}$ have small distances, the meson-meson configuration minimizes the string energy.

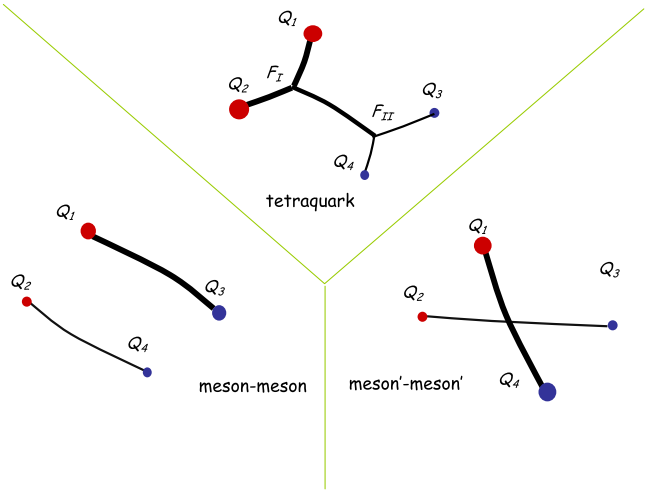

FIG. 1. Triple string flip-flop potential. While the previous string flip-flop potentials choose the minimum of two different meson pair potentials, we consider as well the double Y (or butterfly) potential [2].

4. Previous quark model results with string flip-flop potentials

Tetraquark resonances are quite subtle, since the Fock space of tetraquarks is the same as its decay channels, the meson-meson channels, and moreover, a potential barrier is absent. *A priori* it is not intuitive whether this system may produce resonances.

Nevertheless, there is an argument [57] suggesting multiquarks with angular excitations may gain a centrifugal barrier, leading to narrower decay widths.

With a triple string flip-flop potential, bound states below the threshold for hadronic coupled channels have been found [13,74–76].

On the other hand, the string flip-flip potentials allow fully unitarized studies of resonances [71,72,77]. Utilizing analytical calculations with a double flip-flop harmonic oscillator potential [77], and using the resonating group method again with a double flip-flop confining harmonic oscillator potential [71,72], resonances and bound states have already been predicted. These studies suggest tetraquark bound states or resonances are plausible.

Thus we apply fully unitarized techniques adapted to state of the art potentials, in order to do a quark-model study of tetraquark resonances and bound states.

III. POTENTIAL

A. Ground state string flip-flop potential

We know from lattice computations for static quarks [52–55] that the ground state potential for a system composed of two quarks and two antiquarks is well fitted by a string flip-flop potential,

$$V^0_{FF} = \min(V_{MM}, V_{MM'}, V_{YY}), \tag{3}$$

where, for simplicity, we neglect possible mixings at the transition regions. In Eq. (3), V_{MM} and $V_{MM'}$ are two possible potentials of a pair of mesons, given by the sum of the intrameson potentials $V_{MM}(\mathbf{x}_i) = V_M(|\mathbf{x}_1 - \mathbf{x}_3|) + V_M(|\mathbf{x}_2 - \mathbf{x}_4|)$ and $V_{MM'}(\mathbf{x}_i) = V_M(|\mathbf{x}_1 - \mathbf{x}_4|) + V_M(|\mathbf{x}_2 - \mathbf{x}_3|)$. The intrameson potential is well described by the funnel potential,

$$V_M(\mathbf{r}_{ij}) = K - \frac{\gamma}{r_{ij}} + \sigma r_{ij}, \tag{4}$$

where $r_{ij} = |\mathbf{x}_i - \mathbf{x}_j|$ and where we include a constant term K, the short range Coulomb potential $-\frac{\gamma}{r}$, and the long range confining potential σr. Here we use the indices 1 and 2 to refer to the quarks and 3 and 4 to refer to the antiquarks. $\mathbf{x}_i$ are the positions of the quarks/antiquarks. Moreover, the double Y (or butterfly) potential V_{YY} is

$$V_{YY}(\mathbf{x}_i) = 2K - \sum_{1=i<j}^{4} C_{ij}\frac{\gamma}{r_{ij}} + \sigma L_{\min}(\mathbf{x}_i), \tag{5}$$

where $C_{ij} = 1/2$ for quark-quark and antiquark-antiquark interactions, while $C_{ij} = 1/4$ for quark-antiquark interactions. $L_{\min}$ is the minimal distance linking the four particles,

$$L_{\min}(\mathbf{x}_i) = r_{15} + r_{25} + r_{56} + r_{36} + r_{46}, \tag{6}$$

where 5 and 6 are the indices of the two Fermat-Torricelli-Steiner points [13,74,78] of the tetraquark. We compute the position of these two points with the numerical technique of Ref. [78]. This potential generalizes the earlier string flip-flop potential models by introducing a third possible branch in the potential where the four particles are all linked by a confining string.

B. Color states

Moreover, Refs. [79–83] have pointed out that we also need a potential for color excited states; otherwise there would be solutions that would not respect color confinement.

With two quarks and two antiquarks, two linearly independent color singlets can be constructed. Different color bases can be used, but we find it more convenient (rather than choosing a basis composed by singlet-singlet and octet-octet, or including the triplet-antitriplet) to have a color basis corresponding to the two possible asymptotic meson-meson systems MM and MM'. These two color states are

$$|\mathcal{C}_I\rangle \equiv |\mathbf{1}_{13}\mathbf{1}_{24}\rangle = \frac{1}{3}\delta_{c_1\bar{c}_3}\delta_{c_2\bar{c}_4}|c_1c_2\bar{c}_3\bar{c}_4\rangle,$$
$$|\mathcal{C}_{II}\rangle \equiv |\mathbf{1}_{14}\mathbf{1}_{23}\rangle = \frac{1}{3}\delta_{c_1\bar{c}_4}\delta_{c_2\bar{c}_3}|c_1c_2\bar{c}_3\bar{c}_4\rangle. \tag{7}$$

Notice these two states are not orthogonal,

$$\langle \mathbf{1}_{13}\mathbf{1}_{24}|\mathbf{1}_{14}\mathbf{1}_{23}\rangle = \frac{1}{3}. \tag{8}$$

An orthogonal basis can be constructed by considering the antisymmetric antitriplet-triplet and symmetric sextet-antisextet color combinations of these two states,

$$|\bar{\mathbf{3}}_{12}\mathbf{3}_{34}\rangle = \sqrt{\frac{3}{4}}(|\mathbf{1}_{13}\mathbf{1}_{24}\rangle - |\mathbf{1}_{14}\mathbf{1}_{23}\rangle),$$
$$|\mathbf{6}_{12}\bar{\mathbf{6}}_{34}\rangle = \sqrt{\frac{3}{8}}(|\mathbf{1}_{13}\mathbf{1}_{24}\rangle + |\mathbf{1}_{14}\mathbf{1}_{23}\rangle), \tag{9}$$

and inversely,

$$|\mathbf{1}_{13}\mathbf{1}_{24}\rangle = \sqrt{\frac{2}{3}}|\mathbf{6}_{12}\bar{\mathbf{6}}_{34}\rangle + \frac{1}{\sqrt{3}}|\bar{\mathbf{3}}_{12}\mathbf{3}_{34}\rangle,$$
$$|\mathbf{1}_{14}\mathbf{1}_{23}\rangle = \sqrt{\frac{2}{3}}|\mathbf{6}_{12}\bar{\mathbf{6}}_{34}\rangle - \frac{1}{\sqrt{3}}|\bar{\mathbf{3}}_{12}\mathbf{3}_{34}\rangle. \tag{10}$$

We also introduce two other useful color states, in which quarks and antiquarks form two $SU(3)$ octets while we globally still have a color singlet,

$$|\mathbf{8}_{13}\mathbf{8}_{24}\rangle = \frac{1}{16}\lambda^a_{c_1\bar{c}_3}\lambda^a_{c_2\bar{c}_4}|c_1c_2\bar{c}_3\bar{c}_4\rangle,$$
$$|\mathbf{8}_{14}\mathbf{8}_{23}\rangle = \frac{1}{16}\lambda^a_{c_1\bar{c}_4}\lambda^a_{c_2\bar{c}_3}|c_1c_2\bar{c}_3\bar{c}_4\rangle. \tag{11}$$

These states are important, because of the property

$$\langle \mathbf{8}_{13}\mathbf{8}_{24}|\mathbf{1}_{13}\mathbf{1}_{24}\rangle = 0,$$
$$\langle \mathbf{8}_{14}\mathbf{8}_{23}|\mathbf{1}_{14}\mathbf{1}_{23}\rangle = 0, \tag{12}$$

which will be used later. Again, while we define six different color states with singlets, octets, triplets, and sextets, only two of them are necessary to describe the color state of the system, since there are only two independent color singlets.

C. Completing the color dependent potential

Since we have two independent color singlets, the potential must be given by a 2×2 matrix that can be reconstructed by knowing its eigenvalues v_i and eigenvectors $|u_i\rangle$

$$V = v_0|u_0\rangle\langle u_0| + v_1|u_1\rangle\langle u_1|. \tag{13}$$

Note that both the eigenvalues and the eigenvectors depend on the quark positions.

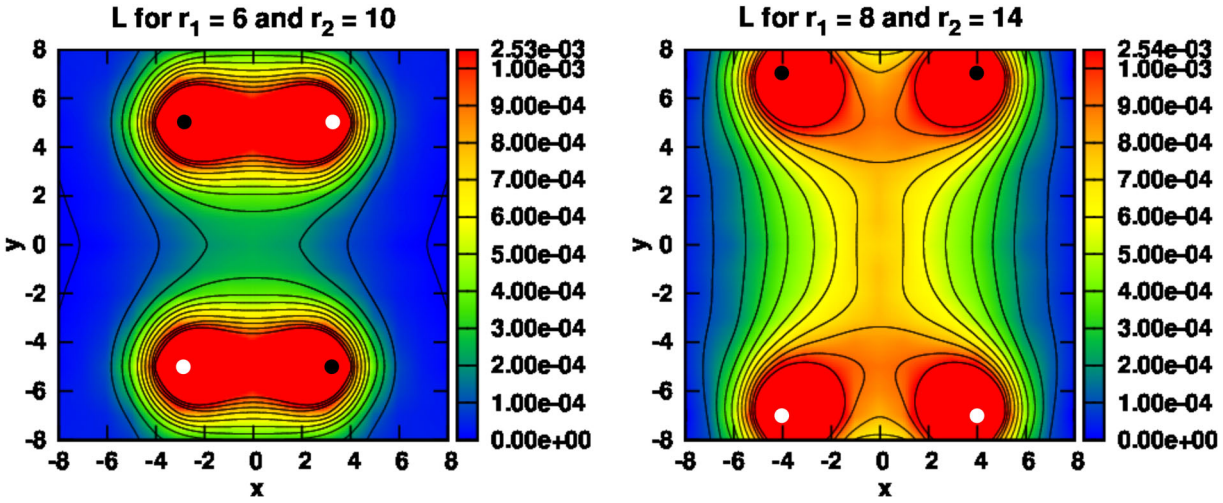

(a) Meson-meson groundstate flux tube (b) Tetraquark groundstate flux tube

FIG. 2. Lagrangian density plots for static quark-quark-antiquark-antiquark flux ground state tubes computed in lattice QCD [55]. The density and the coordinates are in lattice spacing units [55]. Three different flux tubes occur for different geometries of the four-body system.

The lowest eigenvalue of the matrix should correspond to V_{FF} defined in Eq. (3), while the corresponding eigenvectors $|u_0\rangle$ are the following:

(i) when $V_{FF} = V_{MM}$, we have $|u_0\rangle = |\mathbf{1}_{13}\mathbf{1}_{24}\rangle$;
(ii) when $V_{FF} = V_{MM'}$, $|u_0\rangle = |\mathbf{1}_{14}\mathbf{1}_{23}\rangle$;
(iii) when $V_{FF} = V_{YY}$, $|u_0\rangle = |\bar{\mathbf{3}}_{12}\mathbf{3}_{34}\rangle$.

The eigenvector $|u_1\rangle$ of the color excited potential must be orthogonal to $|u_0\rangle$ since the potential has to be Hermitian. So, in the three cases, we have the following eigenvectors:

(i) when $V_{FF} = V_{MM}$, $|u_1\rangle = |\mathbf{8}_{13}\mathbf{8}_{24}\rangle$;
(ii) when $V_{FF} = V_{MM'}$, $|u_1\rangle = |\mathbf{8}_{14}\mathbf{8}_{23}\rangle$;
(iii) when $V_{FF} = V_{YY}$, $|u_1\rangle = |\mathbf{6}_{12}\bar{\mathbf{6}}_{34}\rangle$.

To complete the construction of the potential matrix, we only need to know the highest eigenvalue. In the lattice QCD results of Refs. [55,82], as illustrated in Figs. 2 and 3, in the transition region, are consistent with an exchange between the ground state and the first excited state. Namely, in region A (where V_A is the ground state) close to the transition to region B (where V_B is the ground state), the ground state's potential is $v_0 = V_A$ and the first excited state $v_1 = V_B$. When we enter region B, then we have $v_0 = V_B$ and $v_1 = V_A$. This way, the first excited state should be the second lowest of the three potentials close to the transitions. We assume that this result is valid in general, i.e.,

$$v_1 = \min[\max(V_{MM}, V_{MM'}), \max(V_{MM}, V_{YY}), \max(V_{MM'}, V_{YY})]. \tag{14}$$

Joining all this information into a single equation, the potential is

$$\begin{aligned} V = {} & \Theta(V_{MM} - V_{YY})\Theta(V_{MM'} - V_{YY})(V_{YY}|\bar{\mathbf{3}}_{12}\mathbf{3}_{34}\rangle\langle\bar{\mathbf{3}}_{12}\mathbf{3}_{34}| + \min(V_{MM}, V_{MM'})|\mathbf{6}_{12}\bar{\mathbf{6}}_{34}\rangle\langle\mathbf{6}_{12}\bar{\mathbf{6}}_{34}|) \\ & + \Theta(V_{YY} - V_{MM})\Theta(V_{MM'} - V_{MM})(V_{MM}|\mathbf{1}_{13}\mathbf{1}_{24}\rangle\langle\mathbf{1}_{13}\mathbf{1}_{24}| + \min(V_{YY}, V_{MM'})|\mathbf{8}_{13}\mathbf{8}_{24}\rangle\langle\mathbf{8}_{13}\mathbf{8}_{24}|) \\ & + \Theta(V_{YY} - V_{MM'})\Theta(V_{MM} - V_{MM'})(V_{MM'}|\mathbf{1}_{14}\mathbf{1}_{23}\rangle\langle\mathbf{1}_{14}\mathbf{1}_{23}| + \min(V_{YY}, V_{MM})|\mathbf{8}_{14}\mathbf{8}_{23}\rangle\langle\mathbf{8}_{14}\mathbf{8}_{23}|), \end{aligned} \tag{15}$$

where Θ is the Heaviside step function.

D. Other models

For comparison, we also use two other models. One of them is similar to this color structure dependent triple flip-flop model, but with the double Y sector removed from the potential. So, the ground state's potential is just

$$v_0 = \min(V_{MM}, V_{MM'}), \tag{16}$$

and the excited state is

$$v_1 = \max(V_{MM}, V_{MM'}), \tag{17}$$

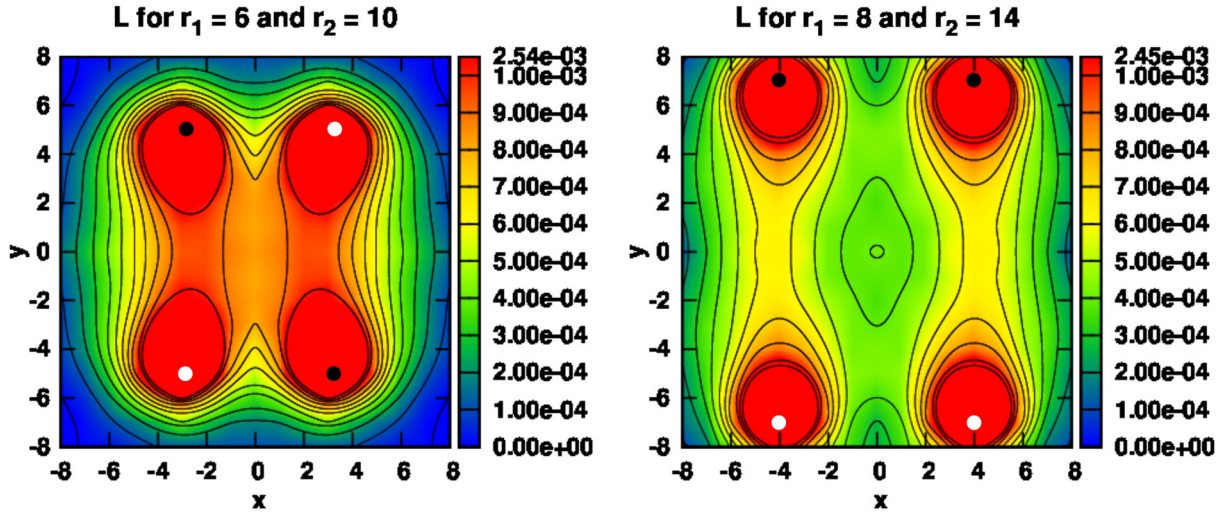

(a) Meson-meson excited flux tube (b) Tetraquark excited flux tube

FIG. 3. Lagrangian density plots for static quark-quark-antiquark-antiquark first excitation flux tubes computed in lattice QCD [55]. The density and the coordinates are in lattice spacing units [55]. We show the first excitation of the different ground state flux tubes shown in Fig. 2. In (a) the excitation of a meson-meson flux tube is similar to the other meson-meson flux tube. In (b) the excitation of a tetraquark flux tube is similar to a meson-meson flux tube.

with the corresponding eigenvectors being constructed the same way as before.

This potential is then given by

$$\begin{aligned} V = {} & \Theta(V_{MM'} - V_{MM})(V_{MM}|\mathbf{1}_{13}\mathbf{1}_{24}\rangle\langle\mathbf{1}_{13}\mathbf{1}_{24}| \\ & + V_{MM'}|\mathbf{8}_{13}\mathbf{8}_{24}\rangle\langle\mathbf{8}_{13}\mathbf{8}_{24}|) \\ & + \Theta(V_{MM} - V_{MM'})(V_{MM}|\mathbf{1}_{14}\mathbf{1}_{23}\rangle\langle\mathbf{1}_{14}\mathbf{1}_{23}| \\ & + V_{MM'}|\mathbf{8}_{14}\mathbf{8}_{23}\rangle\langle\mathbf{8}_{14}\mathbf{8}_{23}|). \end{aligned} \tag{18}$$

A third model we also compare with is the colorless double flip-flop. In this model, the potential is simply given by

$$V = \min(V_{MM}, V_{MM'}). \tag{19}$$

This potential does not depend on the color degrees of freedom of the system and so is not physically complete. However, this model, and its extension including the double Y sector, has been used by several authors [71,72,77]. It can be interpreted as the limit of a color structure dependent model, when the two color eigenstates of the potential are degenerate ($v_0 = v_1$).

IV. OUR UNITARY TECHNIQUE TO SOLVE THE MESON-MESON SCATTERING AND FIND TETRAQUARK BOUND STATES AND RESONANCES

A. Meson-meson scattering equation

Let us start with the microscopic Hamiltonian,

$$\hat{H} = \hat{T}_Q + \hat{V}_Q, \tag{20}$$

where the Q subscript means we are dealing with the kinetic and potential energy of the quarks and not of the mesons. Folding the Hamiltonian, left and right, with the two $\mathcal{C}_A$ color states, we get the Schrödinger equation

$$(g_{AB}T_Q + V^Q_{AB})\Psi^B = E g_{AB}\Psi^B, \tag{21}$$

where

$$g = \begin{pmatrix} 1 & 1/3 \\ 1/3 & 1 \end{pmatrix}. \tag{22}$$

In matrix form the Hamiltonian is given by

$$H_{AB} = \begin{pmatrix} T_Q + V_{I,I} & \frac{1}{3}T_Q + V_{I,II} \\ \frac{1}{3}T_Q + V_{II,I} & T_Q + V_{II,II} \end{pmatrix}_{AB}. \tag{23}$$

Our goal is the study of meson-meson scattering because the mesons (not the quarks) are the asymptotic states of the theory. We thus need the meson kinetic energy operator to show explicitly in the Schrödinger equation. The kinetic energy of the meson-meson systems for each sector is

$$\begin{aligned} T_{MM} &= T_Q + V_{MM}, \\ T_{MM'} &= T_Q + V_{MM'}. \end{aligned} \tag{24}$$

Since these two operators are different and the asymptotic meson-meson states are not orthogonal, we must solve the problem of finding the kinetic energy and potential energy operators for the interacting two meson states.

A naive guess would be to consider the kinetic energy operator,

$$\begin{pmatrix} 1 & \frac{1}{3} \\ \frac{1}{3} & 1 \end{pmatrix} \begin{pmatrix} T_{MM} & \\ & T_{MM'} \end{pmatrix}, \tag{25}$$

to allow the MM and MM' components to decouple for this operator, since the g matrix would cancel. However, this operator is not Hermitian as can easily be seen by evaluating the matrix product.

To solve this, we consider the Hermitian part of Eq. (25),

$$\frac{1}{2} g \begin{pmatrix} T_{MM} & \\ & T_{MM'} \end{pmatrix} + \frac{1}{2} \begin{pmatrix} T_{MM} & \\ & T_{MM'} \end{pmatrix} g, \tag{26}$$

as the kinetic energy operator of our scattering problem. Proceeding, we decompose the Hamiltonian of (23) into two Hermitian operators

$$H = T_S + V_S \tag{27}$$

given by

$$T_S = \begin{pmatrix} T_{MM} & \frac{T_{MM}+T_{MM'}}{6} \\ \frac{T_{MM}+T_{MM'}}{6} & T_{MM'} \end{pmatrix} \tag{28}$$

and

$$V_S = \begin{pmatrix} V_{I,I} - V_{MM} & V_{I,II} - \frac{V_{MM}+V_{MM'}}{6} \\ V_{II,I} - \frac{V_{MM}+V_{MM'}}{6} & V_{II,II} - V_{MM'} \end{pmatrix}. \tag{29}$$

This is the Hamiltonian operator we use to study the meson-meson scattering problem.

Dropping the S subscript, we get the Schrödinger equation,

$$T_{AB}\Psi^B + V_{AB}\Psi^B = E g_{AB}\Psi^B, \tag{30}$$

where we expand the components of the wave function Ψ^A as

$$\begin{aligned} \Psi^I &= \sum_i \Phi_j^I(\boldsymbol{\rho}_{13}, \boldsymbol{\rho}_{24})\psi_i^I(\mathbf{r}_{1324}), \\ \Psi^{II} &= \sum_i \Phi_j^{II}(\boldsymbol{\rho}_{14}, \boldsymbol{\rho}_{23})\psi_i^{II}(\mathbf{r}_{1423}), \end{aligned} \tag{31}$$

and where we define as four-body Jacobi coordinates,

$$\begin{aligned} \boldsymbol{\rho}_{13} &= \mathbf{x}_1 - \mathbf{x}_3, \\ \boldsymbol{\rho}_{24} &= \mathbf{x}_2 - \mathbf{x}_4, \\ \mathbf{r}_{1324} &= \frac{m_1\mathbf{x}_1 + m_3\mathbf{x}_3}{m_1 + m_3} - \frac{m_2\mathbf{x}_2 + m_4\mathbf{x}_4}{m_2 + m_4}, \\ \boldsymbol{\rho}_{14} &= \mathbf{x}_1 - \mathbf{x}_4, \\ \boldsymbol{\rho}_{23} &= \mathbf{x}_2 - \mathbf{x}_3, \\ \mathbf{r}_{1423} &= \frac{m_1\mathbf{x}_1 + m_4\mathbf{x}_4}{m_1 + m_4} - \frac{m_2\mathbf{x}_2 + m_3\mathbf{x}_3}{m_2 + m_3}. \end{aligned} \tag{32}$$

We denote as Φ_i^A the eigenfunctions of the Hamiltonian of the two noninteracting mesons,

$$(T_A + V_A)\Phi_i^A = E_{0i}\Phi_i^A. \tag{33}$$

The eigenfunctions must comply with

$$\lim_{\rho_1\to\infty} \Phi_i^A(\boldsymbol{\rho}_1, \boldsymbol{\rho}_2) = \lim_{\rho_2\to\infty} \Phi_i^A(\boldsymbol{\rho}_1, \boldsymbol{\rho}_2) = 0, \tag{34}$$

because the quarks in each meson are confined.

Substituting Eq. (31) into Eq. (30) and integrating the confined degrees of freedom, (i.e., the $\boldsymbol{\rho}_i$ coordinates), we obtain the multichannel equation,

$$\hat{T}_{\alpha\beta}\psi^\beta + \hat{V}_{\alpha\beta}\psi^\beta = E\hat{g}_{\alpha\beta}\psi^\beta. \tag{35}$$

Here, we employ Greek indices to denote both the color structure and the internal quantum numbers.

The operators $\hat{T}_{\alpha\beta}$, $\hat{V}_{\alpha\beta}$, and $\hat{g}_{\alpha\beta}$ are local between states with the same color structure but are nonlocal between states with different color structures. Let us now analyze in detail the nonlocal operators. Consider the nondiagonal term of the g matrix, folding it with Ψ^I and Ψ^{II},

$$\begin{aligned} \langle\Psi^I|g_{I,II}|\Psi^{II}\rangle = \frac{1}{3}\sum_{ij}\int & d^3\boldsymbol{\rho}_{13} d^3\boldsymbol{\rho}_{24} d^3\mathbf{r}_{1324} \\ & \times \Phi_i^I(\boldsymbol{\rho}_{13}, \boldsymbol{\rho}_{24})^* \psi^I(\mathbf{r}_{1324})^* \\ & \times \Phi_j^{II}(\boldsymbol{\rho}_{14}, \boldsymbol{\rho}_{23})\psi^{II}(\mathbf{r}_{1423}). \end{aligned} \tag{36}$$

Changing the integration variables to $\mathbf{r}_{1324}$, $\mathbf{r}_{1423}$, and

$$\mathbf{r}_{1234} = \frac{m_1\mathbf{x}_1 + m_2\mathbf{x}_2}{m_1 + m_2} - \frac{m_3\mathbf{x}_3 + m_4\mathbf{x}_4}{m_3 + m_4}, \tag{37}$$

in order to isolate functions of $\mathbf{r}_{1324}$ and $\mathbf{r}_{1423}$, the integral becomes

$$\frac{1}{3}\int d^3\mathbf{r}_{1324} d^3\mathbf{r}_{1423} \psi_i^I(\mathbf{r}_{1324})^* \gamma_{ij}(\mathbf{r}_{1324}, \mathbf{r}_{1423})\psi_j^{II}(\mathbf{r}_{1423}).$$

The function $\gamma_{ij}(\mathbf{r}_{1324}, \mathbf{r}_{1423})$ is given by

$$\gamma_{ij} = \Delta \int d^3\mathbf{r}_{1234} \Phi_i^I(\boldsymbol{\rho}_{13},\boldsymbol{\rho}_{24})^* \Phi_j^{II}(\boldsymbol{\rho}_{14},\boldsymbol{\rho}_{23}), \quad (38)$$

where

$$\Delta = \left(\frac{M_{12}M_{34}M_{13}M_{24}M_{14}M_{23}}{2m_1m_2m_3m_4M^2}\right)^3, \quad (39)$$

with $M_{ij} = m_i + m_j$ and $M = \sum_i m_i$. In this way, since $\hat{g}$ acts on a function as

$$\hat{g}_{\alpha\beta}\psi_\beta = \int d^3\mathbf{r}_\beta g_{\alpha\beta}(\mathbf{r}_\alpha, \mathbf{r}'_\beta)\psi^\beta(\mathbf{r}'_\beta), \quad (40)$$

we have

$$\begin{aligned} g_{Ii,Ij}(\mathbf{r}_{1324}, \mathbf{r}'_{1324}) &= \delta_{ij}\delta^3(\mathbf{r}_{1324} - \mathbf{r}'_{1324}), \\ g_{Ii,IIj}(\mathbf{r}_{1324}, \mathbf{r}'_{1423}) &= \frac{1}{3}\gamma_{ij}(\mathbf{r}_{1324}, \mathbf{r}'_{1423}), \\ g_{IIi,Ij}(\mathbf{r}_{1423}, \mathbf{r}'_{1324}) &= \frac{1}{3}\gamma_{ji}(\mathbf{r}'_{1324}, \mathbf{r}_{1423})^*, \\ g_{IIi,IIj}(\mathbf{r}_{1324}, \mathbf{r}'_{1423}) &= \delta_{ij}\delta^3(\mathbf{r}_{1423} - \mathbf{r}'_{1423}). \end{aligned} \quad (41)$$

The potential $\hat{V}$ has a similar structure,

$$\begin{aligned} V_{Ai,Aj}(\mathbf{r}_A, \mathbf{r}'_A) &= V_{ij}^{AA}(\mathbf{r}_A)\delta^3(\mathbf{r}_A - \mathbf{r}'_A), \\ V_{Ii,IIj}(\mathbf{r}_{1324}, \mathbf{r}'_{1423}) &= v_{ij}(\mathbf{r}_{1324}, \mathbf{r}'_{1423}), \\ V_{IIi,Ij}(\mathbf{r}_{1324}, \mathbf{r}'_{1324}) &= v_{ji}^*(\mathbf{r}'_{1324}, \mathbf{r}_{1423}), \end{aligned} \quad (42)$$

with

$$\begin{aligned} V_{ij}^{II} &= \int d^3\boldsymbol{\rho}_{13} d^3\boldsymbol{\rho}_{24} \Phi_i^I(\boldsymbol{\rho}_{13},\boldsymbol{\rho}_{24})^* (V_{I,I} - V_I)\Phi_j^I(\boldsymbol{\rho}_{13},\boldsymbol{\rho}_{24}), \\ V_{ij}^{IIII} &= \int d^3\boldsymbol{\rho}_{14} d^3\boldsymbol{\rho}_{23} \Phi_i^I(\boldsymbol{\rho}_{14},\boldsymbol{\rho}_{23})^* (V_{II,II} - V_{II})\Phi_j^I(\boldsymbol{\rho}_{14},\boldsymbol{\rho}_{23}), \\ v_{ij} &= \Delta \int d^3\mathbf{r}_{1234} \\ &\quad \times \Phi_i^I(\boldsymbol{\rho}_{13},\boldsymbol{\rho}_{24})^* \left(V_{I,II} - \frac{V_I + V_{II}}{6}\right)\Phi_j^{II}(\boldsymbol{\rho}_{14},\boldsymbol{\rho}_{23}). \end{aligned} \quad (43)$$

Note, because of Eq. (34), both γ_{ij} and v_{ij} have the property

$$\lim_{r_1\to\infty} \gamma_{ij}(\mathbf{r}_1, \mathbf{r}_2) = \lim_{r_2\to\infty} \gamma_{ij}(\mathbf{r}_1, \mathbf{r}_2) = 0. \quad (44)$$

The color structure preserving elements of $\hat{T}$ are just common kinetic energy operators,

$$\hat{T}_{Ai,Aj} = \delta_{ij}\left(E_{0i}^A - \frac{\hbar^2}{2\mu_i^A}\nabla_A^2\right), \quad (45)$$

while the elements between states with different color structures are given by

$$\begin{aligned} \hat{T}_{Ii,IIj} &= \frac{1}{6}\gamma_{ij}(\mathbf{r}_{1324}, \mathbf{r}_{1423})\left(E_{0i}^{II} - \frac{\hbar^2}{2\mu_j^{II}}\nabla_{1423}^2\right) \\ &\quad + \frac{1}{6}\left(E_{0i}^I - \frac{\hbar^2}{2\mu_j^I}\nabla_{1324}^2\right)\gamma_{ij}(\mathbf{r}_{1324}, \mathbf{r}_{1423}). \end{aligned} \quad (46)$$

B. T matrix

We now construct the T matrix. The T matrix poles correspond to the bound states and resonances of the system. Bound states correspond to real poles, and we check our code by comparing them with the bound state energies obtained solving the Schrödinger equation. To find the resonances we search for the T matrix poles on the complex plane. The imaginary part of the pole is $-i\Gamma/2$, where Γ is the total decay width of the resonance.

Since $\hat{T}$, $\hat{V}$, and $\hat{g}$ are Hermitian, we apply the continuity equation (for stationary states),

$$\Im[\psi^{\alpha*}\hat{T}_{\alpha\beta}\psi^\beta] = 0, \quad (47)$$

or, in integral form,

$$\sum_\alpha \Phi_\alpha = 0, \quad (48)$$

where the fluxes Φ_α are

$$\Phi_\alpha = \sum_\beta \int d^3\mathbf{r}_\alpha 2\Im[\psi^\alpha \hat{T}_{\alpha\beta}\psi^\beta], \quad (49)$$

and the 2 factor is to get the usual flux definition.

Using the structure of $\hat{T}$ and the asymptotic behavior of γ_{ij} given by Eqs. (45), (46), and (44) we can easily prove that nondiagonal terms on Eq. (47) do not contribute to the fluxes Φ_α. In this way, we get

$$\Phi_\alpha = \int dS\hat{\mathbf{n}}_\alpha \cdot \frac{\hbar}{2i\mu_\alpha}(\psi^{\alpha*}\nabla_\alpha\psi^\alpha - \psi^\alpha\nabla_\alpha\psi^{\alpha*}). \quad (50)$$

Expanding each component ψ^α as

$$\psi^\alpha(\mathbf{r}) = \frac{u^\alpha(r)}{r}Y_{lm}(\theta_\alpha, \varphi_\alpha), \quad (51)$$

and taking the $r \to \infty$ limit, we obtain

$$\Phi^\alpha = \lim_{r\to\infty}\frac{\hbar}{\mu_\alpha}\Im\left[u^{\alpha*}\frac{du^\alpha}{dr}\right]. \quad (52)$$

To compute the T matrix of the system, we first note that the wave function can be expanded as

$$u^\alpha(r) = \sum_i c_i u_i^\alpha(r), \tag{53}$$

where each $u_i^\alpha(r)$ can be decomposed into two parts,

$$u_i^\alpha(r) = u_{0i}^\alpha(r) + v_i^\alpha(r). \tag{54}$$

The function $u_{0i}^\alpha(r)$ comes from the eigenfunction ψ_0^α of $\hat{T}$ and has the asymptotic limit

$$u_{0i}^\alpha(r) \to A_{i\alpha}\sqrt{\frac{\mu_\alpha}{k_\alpha}}\sin\left(k_\alpha r - \frac{l_\alpha\pi}{2} + \varphi_{i\alpha}\right), \tag{55}$$

where the term $\varphi_{i\alpha}$ appears because $\hat{T}$ mixes the different channels, while $v_{i\alpha}$ is the scattered component and has the asymptotic behavior

$$v_i^\alpha \to f_{i\alpha} e^{ik_\alpha r - \frac{l_\alpha\pi}{2}}. \tag{56}$$

The u_{0i}^α can be chosen to form an orthonormal basis,

$$\langle u_{0i}|u_{0j}\rangle = \frac{\pi}{2}\delta(E_i - E_j)\delta_{ij}, \tag{57}$$

which imposes that the parameters $A_{i\alpha}$ and $\varphi_{i\alpha}$ must comply with the relation

$$\sum_\alpha A_{i\alpha}A_{j\alpha}\cos(\varphi_{i\alpha} - \varphi_{j\alpha}) = \delta_{ij}. \tag{58}$$

Replacing Eqs. (53) and (56) in Eq. (52), we get

$$\sum_\alpha \sqrt{\frac{k_\alpha}{\mu_\alpha}}\frac{A_{i\alpha}e^{-i\varphi_{i\alpha}}f_{j\alpha} - A_{j\alpha}e^{-i\varphi_{j\alpha}}f_{i\alpha}}{2i} = \sum_\alpha \frac{k_\alpha}{\mu_\alpha} f_{i\alpha}^* f_{j\alpha}. \tag{59}$$

We note that the left side of this equation has the form consistent with

$$\frac{T_{ij} - T_{ji}^*}{2i} \equiv \left(\frac{T - T^\dagger}{2i}\right)_{ij}, \tag{60}$$

which is consistent with the definition for the T matrix,

$$T_{ij} = \sum_\alpha \sqrt{\frac{k_\alpha}{\mu_\alpha}} A_{i\alpha} e^{-i\varphi_{i\alpha}} f_{j\alpha}. \tag{61}$$

To verify Eq. (61) is correct, we use the relation

$$\sum_k A_{k\alpha}A_{k\beta}e^{i(\varphi_{k\alpha} - \varphi_{k\beta})} = \delta_{\alpha\beta}, \tag{62}$$

which is proved using the completeness relation,

$$\sum_n |\psi_n\rangle\langle\psi_n| = \hat{1}, \tag{63}$$

of the eigenvectors of the kinetic energy $\hat{T}$ operator. With Eq. (62), we calculate $T^\dagger T$, and indeed we prove that it is equal to the right side of Eq. (59),

$$T^\dagger T = \sum_\alpha \frac{k_\alpha}{\mu_\alpha} f_{i\alpha}^* f_{j\alpha}. \tag{64}$$

Therefore, by the definition of T and the previous relation, we can write Eq. (59) as

$$\mathrm{Im}T = T^\dagger T, \tag{65}$$

thus proving we comply with the unitarity of the S matrix defined by $S = 1 + 2iT$.

C. Identical quarks and identical antiquarks

So far, our framework is general for four-quark systems. We now specialize our study to a system of two identical quarks and two identical antiquarks, which is our case study.

The total wave function must be antisymmetric under the quark-exchange P_{12} and antiquark exchange P_{34},

$$\begin{aligned} P_{12}\Psi &= -\Psi, \\ P_{34}\Psi &= -\Psi. \end{aligned} \tag{66}$$

Given a generic wave function Ψ we construct a completely antisymmetric one, Ψ_A, by applying a projection operator

$$\Psi_A = \mathcal{N}(1 - P_{12} - P_{34} + P_{12}P_{34})\Psi. \tag{67}$$

In this work, our Hamiltonian is spin independent, and so we ignore spin effects in the dynamics of the system. With this approximation, the spin part of the wave function factorizes, and we can neglect its existence for everything except for the symmetry of the wave function. Now, let us consider the wave function,

$$\Psi = \phi_\alpha(\boldsymbol{\rho}_{13})\phi_\beta(\boldsymbol{\rho}_{24})\psi(\mathbf{r}_{1324})\mathcal{C}_I\Sigma, \tag{68}$$

where $\mathcal{C}_I$ is the color part and Σ is the spin part of the wave function, and where ψ has parity

$$\psi(-\mathbf{r}) = (-1)^{L_r}\psi(\mathbf{r}). \tag{69}$$

To impose the correct antisymmetry, we use Eq. (67) and we obtain the wave function,

$$\Psi_A = \mathcal{N}[\phi_\alpha(\boldsymbol{\rho}_{13})\phi_\beta(\boldsymbol{\rho}_{24})\psi(\mathbf{r}_{1324})\mathcal{C}_I - (-1)^{1+S_{12}+L_r}\phi_\alpha(\boldsymbol{\rho}_{23})\phi_\beta(\boldsymbol{\rho}_{14})\psi(\mathbf{r}_{1423})\mathcal{C}_{II} - (-1)^{1+S_{34}}\phi_\alpha(\boldsymbol{\rho}_{14})\phi_\beta(\boldsymbol{\rho}_{23})\psi(\mathbf{r}_{1423})\mathcal{C}_{II} + (-1)^{S_{12}+S_{34}+L_r}\phi_\alpha(\boldsymbol{\rho}_{24})\phi_\beta(\boldsymbol{\rho}_{13})\psi(\mathbf{r}_{1324})\mathcal{C}_I]\Sigma, \tag{70}$$

where S_{12} and S_{34} are, respectively, the spins of the 12 and 34 diquarks. We assume that Σ is an eigenfunction of both $\hat{S}_{12}$ and $\hat{S}_{34}$. This is consistent with our approximation of neglecting all spin related interactions, which implies that all spin operators commute trivially with the Hamiltonian. Defining

$$s \equiv (-1)^{S_{12}+S_{34}+L_r}, \qquad \xi \equiv (-1)^{S_{34}}, \tag{71}$$

Ψ_A simplifies to

$$\Psi_A = \mathcal{N}[\Phi(\boldsymbol{\rho}_{13},\boldsymbol{\rho}_{24})\psi(\mathbf{r}_{1324})\mathcal{C}_I + \xi\Phi(\boldsymbol{\rho}_{14},\boldsymbol{\rho}_{23})\psi(\mathbf{r}_{1423})\mathcal{C}_{II}]\Sigma, \tag{72}$$

where the function $\Phi(\mathbf{x},\mathbf{y})$ is defined as

$$\Phi(\mathbf{x},\mathbf{y}) = \phi_a(\mathbf{x})\phi_b(\mathbf{y}) + s\phi_a(\mathbf{y})\phi_b(\mathbf{x}) \tag{73}$$

and has the symmetry

$$\Phi(\mathbf{y},\mathbf{x}) = s\Phi(\mathbf{x},\mathbf{y}). \tag{74}$$

Since both $\hat{S}_{12}$ and $\hat{S}_{34}$ are conserved in the nondynamic spin approximation, we diagonalize our Hamiltonian by blocks with fixed values of these two operators. This is done by substituting Eq. (70) in Eq. (35). We obtain the scattering equation

$$\hat{T}_{\alpha\beta}\psi^\beta(\mathbf{r}) + V^D_{\alpha\beta}\psi^\beta(\mathbf{r}) + \xi\int d^3\mathbf{r}' v_{\alpha\beta}(\mathbf{r},\mathbf{r}')\psi^\beta(\mathbf{r}') = E\left(\psi^\alpha + \xi\int d^3\mathbf{r}'\gamma_{\alpha\beta}(\mathbf{r},\mathbf{r}')\psi^\beta(\mathbf{r}')\right). \tag{75}$$

Moreover, the total orbital angular momentum $\hat{L}$ and parity are also conserved. Thus we can determine several quantum numbers for our system. For instance, for $S_{12} = S_{34} = 0$, we only have $J = L$ states. In this case, $\xi = 1$ and $s = (-1)^{L_r}$. For $S_{12} = S_{34} = 1$, we have $\xi = -1$ and still $s = (-1)^{L_r}$. The total angular momentum J can range from $|L-2|$ to $L+2$, as shown in Table I. In Table II we show an example of the channels we use in a particular system.

TABLE I. Quantum numbers of the $qq\bar{Q}\bar{Q}$ system.

S_{12}	S_{34}	ξ	$s(-1)^{L_r}$	J
0	0	+1	+1	L
0	1	−1	−1	$\lvert L-1\rvert$ to $L+1$
1	0	+1	−1	$\lvert L-1\rvert$ to $L+1$
1	1	−1	+1	$\lvert L-2\rvert$ to $L+2$

D. Numerical technique

We consider the intramesonic potential to be of the funnel type, with no other corrections, and the kinetic energy completely nonrelativistic.

Moreover, we neglect all other relativistic effects on our model, such as quark-antiquark annihilation and spin-spin and spin-orbit interactions. Besides, we assume that we are well below the threshold for decay into a baryon-antibaryon system. In this way we can neglect all the baryon-antibaryon channels and consider just the meson-meson ones.

For the potential, we fix its parameters by fitting lowest charmonium and bottomonium to the weighted average mass of the pseudoscalar and vector states

$$\bar{M} = \frac{1}{4}M_{PS} + \frac{3}{4}M_V. \tag{76}$$

We thus use the quark masses $m_c = 1.3$ GeV and $m_b = 4.7$ GeV, together with the parameters $K = 0$, $\gamma = 0.41$, and $\sigma = 0.19$ GeV^2.

It is trivial to compute the meson states with our potential. We calculate the wave functions of the mesons. We use an harmonic oscillator variational basis, where each function is given by

$$\phi^\beta_{nlm}(r,\theta,\varphi) = \sqrt{\frac{2n!\beta^3}{\Gamma(n+l+\frac{3}{2})}}(\beta r)^l \mathrm{L}_n^{l+1/2}(\beta^2 r^2) \times e^{-\frac{1}{2}\beta^2 r^2}Y_{lm}(\theta,\varphi). \tag{77}$$

TABLE II. Scattering channels used in this work for the 0^+ $cc\bar{b}\bar{b}$ system.

n_1	L_1	n_2	L_2	L_r	s
0	0	0	0	0	+1
0	0	0	1	1	−1
0	0	1	0	0	+1
0	0	2	0	2	+1
0	1	0	1	0	+1
0	1	0	1	2	+1
0	0	1	1	1	−1
0	0	0	3	3	−1
1	0	0	1	1	−1
0	0	2	0	0	+1

TABLE III. Masses M_0 of the ground states of the $q\bar{Q}$ mesons used on this work.

m_q[GeV]	$m_{\bar{Q}}$[GeV]	M_0[GeV]
0.4	1.3	2.433
0.7	1.3	2.592
1.0	1.3	2.818
1.3	1.3	3.072
0.4	4.7	5.766
0.7	4.7	5.893
1.0	4.7	6.094
1.3	4.7	6.326

$L_n^{l+1/2}$ are generalized Laguerre polynomials and β is a variational parameter with the value we choose as $\beta = (\frac{4m\sigma}{3\sqrt{\pi}})^{1/3}$. We compute the meson Hamiltonian matrix elements in this basis, and then we diagonalize the matrix. We list the lowest energy meson in Table III.

1. Computation of meson-meson interaction

With the meson eigenfunctions $\phi^{\beta}_{nlm}(r,\theta,\varphi)$, we calculate the local V^{AA}_{ij} and nonlocal v_{ij} parts of the meson-meson potential, defined by Eq. (43) and the nonlocal parts of the metric matrix γ_{ij} defined by Eq. (38). We calculate these seven- (nonlocal) or eight- (local) dimensional integrals using Lebedev quadrature [84] in the angular coordinates and the Gauss-Laguerre quadrature for the radial coordinates.

This is the most numerical intensive part of our study. We thus develop CUDA language parallel codes to compute these multidimensional integrals and run them in our servers with NVIDIA GTX graphics processing units. The resulting functions depend on one radial coordinate in the local case and on two radial coordinates in the nonlocal case. So, in both cases, the functions are evaluated on a nine-dimensional space.

2. Meson-meson scattering

We must solve Eq. (35) to obtain the asymptotic behavior of the wave function and compute the T matrix.

This is done by discretizing the radial scattering coordinates on a finite box. We first solve the "free" equation

$$\hat{T}\Psi_0 = Eg\Psi_0. \tag{78}$$

This is not as simple to solve as it may seem, since we cannot solve this equation separately for each channel, given the form of the kinetic $\hat{T}$ matrix and of the color g matrix, which link all the channels. Our system is more cumbersome than systems where there is only one type of quark combinations in mesons, e.g., only $(q_1\bar{q}_3)(q_2\bar{q}_4)$ and not $(q_1\bar{q}_4)(q_2\bar{q}_3)$ [2].

For each energy, we can generate different wave functions by varying the boundary conditions of the open channels. Note the generated numerical solutions are not yet fully orthogonal, and we still have to orthogonalize them. We stress we must be particularly careful in determining the asymptotic behavior of the functions. We cannot consider the internal product of two wave functions to be just given by the values on the finite box used for numerics,

$$\langle u|v\rangle = \sum_i u_i^* v_i, \tag{79}$$

because, although the two functions u and v are orthogonal in the box, the continuations of them beyond the box $\tilde{u}$ and $\tilde{v}$ are not necessarily orthogonal $\langle\tilde{u}|\tilde{v}\rangle \neq 0$.

Instead, we must utilize an inner product that takes into account the behavior of the wave function continued outside the box. To achieve this, we consider the inner product of two functions to be given by

$$\langle u_i|u_j\rangle = \sum_\alpha A_{i\alpha}A_{j\alpha}\cos(\varphi_{i\alpha}-\varphi_{j\alpha}) \tag{80}$$

in accordance with Eq. (58). The parameters $A_{i\alpha}$ and $\varphi_{i\alpha}$ are given by Eq. (55) and are computed from the value of the wave function components at the boundary of the box.

Having generated our basis of N_{open} (the number of open channels) eigenfunctions of $\hat{T}$ for a given energy, we orthogonalize the basis with the Gram-Schmidt procedure, using the inner product of Eq. (80).

Then, for each function of the orthogonalized basis, we solve the scattering Eq. (35) considering $\Psi_i = \Psi_{0i} + \chi_i$. In this way the equation becomes

$$(\hat{T}+\hat{V})\chi_i = Eg\chi_i - V\Psi_{0i}. \tag{81}$$

We solve this equation numerically by discretizing the position space, using suitable boundary conditions for χ_i. We then calculate the values of $f_{i\alpha}$ from the behavior of $\chi_{i\alpha}$ at the boundary of the box. We evaluate the T matrix utilizing Eq. (61).

3. Finding bound states

To find the bound states of our system we do not need to calculate the T matrix. We directly solve Eq. (35) and search for states with energy smaller than the first threshold.

We solve Eq. (35) with finite differences, discretizing it in a position space box. Naively, one would use Dirichlet boundary conditions, but they are acceptable only if the spatial extent of the bound state is much smaller than the box on which we are solving the equation. When this does not happen, the wave function can become highly distorted by the forced boundary conditions, and the energy can even be moved above the threshold, hiding the nature of the state. In this work, we find some bound states with a very small biding energy. Thus, instead of using Dirichlet boundary conditions, we consider boundary conditions

that depend on the energy and match the expected behavior of the wave functions at large distances.

With this method, we have to solve the matrix equation,

$$[H + F(E)]u = Egu, \tag{82}$$

where $F(E)$ is a matrix that fixes the boundary conditions. This is not a simple eigenvalue problem as the matrix depends on the eigenvalue itself. To solve this equation, we consider it as a root finding problem $\det[H + F(E) - Eg] = 0$ and use Newton's method,

$$x^{(n+1)} = x^{(n)} - \frac{f(x^{(n)})}{f'(x^{(n)})}, \tag{83}$$

to solve it. Applying this method to Eq. (82), we obtain the iteration procedure

$$E^{(n+1)} = E^{(n)} - \frac{1}{\mathrm{Tr}[(H + F(E) - Eg)^{-1}(F'(E) - g)]}, \tag{84}$$

and we use it to calculate the bound state energy. Iteratively, we compute the wave function by solving Eq. (82), which is a simple linear system.

With this numerical method, we find the bound states for the $qq\bar{b}\bar{b}$ systems detailed in Sec. V.

4. Finding resonances

To find the resonances in our $qq\bar{b}\bar{b}$ systems, we extend the T matrix to the complex energy plane. Resonances correspond to complex poles of the S (or T) matrix. Thus, to find resonances, we search for zeros of the quantity,

$$y(E) = 1/\mathrm{Tr(T)}. \tag{85}$$

Indeed, at a pole, the T matrix is divergent and so is its trace; therefore $y(E) = 0$. Numerically, to find a T matrix pole, we apply Newton's method to Eq. (85).

V. RESULTS

A. Bound states

We apply the method detailed in Sec. IV to find bound states in the $qq\bar{b}\bar{b}$ system. We study different values of the light quark mass, for angular momentum $L = 0$, and we are able to find bound states for quark masses ranging from $m_q = 0.4$ to $m_q = 1.3$ GeV. We find the bound states with $s(-1)^{L_r} = +1$, $\xi = +1$, listed in Table IV. The bound state is weakly bound for $m_q = 1.3$ GeV, i.e., for the charm mass (see Table II for the respective channels), and becomes more strongly bound as m_q decreases. Wave functions for the first dominant channel are given in Fig. 4.

Now, comparing Table I, these bound states have $S_{12} = S_{34} = 0$, and hence $L = 0$ and $J = 0$. If the lightest quarks are u and d quarks, we also have to consider the isospin symmetry, contributing an additional $(-1)^{I_{12}+1}$ factor for the P_{12} symmetry of the wave function. In this way, the previous results are unchanged if $I_{12} = 1$. However, if $I = 0$, the flavor wave function is antisymmetric, and so the spin wave function has to change its symmetry in order for the total wave function to be completely antisymmetric. So, for $I_{12} = 0$, we also have $S_{12} = 1$, and hence $S = 1$ and $J = 1$.

TABLE IV. Bound states in the system $qq\bar{b}\bar{b}$ with $L = 0$ and $P = +$. We use $m_b = 4.7$ GeV. The radius presented here is estimated from the long range exponential decay of the lowest wave function component $\sim e^{-qr}$.

m_q[GeV]	B[MeV]	$R = \frac{1}{q_0}$[fm]
1.30	0.4	4.12
1.00	1.4	2.24
0.70	4.2	1.31
0.40	20.3	0.61

To summarize, we obtain tetraquark bound states on the $qq\bar{b}\bar{b}$ system, with quantum numbers 0^+ for s and c quarks, or light quarks with $I_{12} = 1$. For light quarks with $I_{12} = 0$, we obtain bound states with quantum numbers 1^+.

We also tried to find bound states for the $qq\bar{c}\bar{c}$ system, but we were unable to find them when the lightest quarks have constituent masses equal to or larger than the ones of light quarks $m_q \geq 400$ MeV.

B. Resonances

We also compute the T matrix and search for poles in the S matrix, for the $qq\bar{b}\bar{b}$ system.

For the $cc\bar{b}\bar{b}$ system with $L = 0$, $P = +$, and $\xi = +1$, we find several poles of the S matrix in the complex energy plane, corresponding to resonances between all threshold

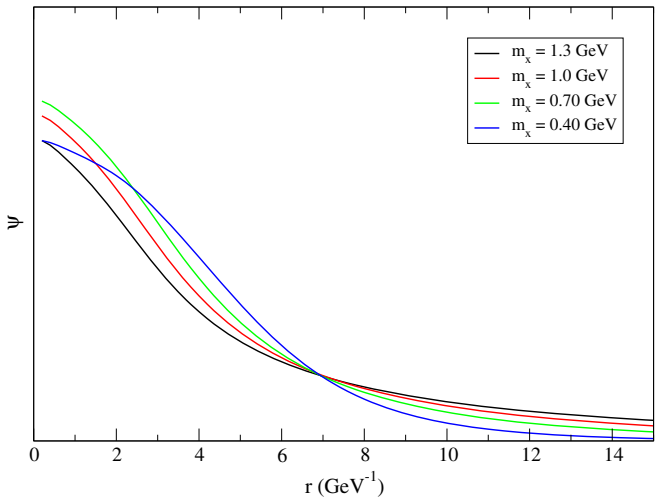

FIG. 4. Wave functions of the bound states we find in the $qq\bar{b}\bar{b}$ system.

TABLE V. Resonances in the 0^+ $cc\bar{b}\bar{b}$ system, with $\xi = +1$, for different numbers of open channels N_{open}. E_n and E_{n+1} are the energies of the two thresholds.

N_{open}	E[GeV]	E_n	E_{n+1}
1	$12.7011 - 0.2293i$	12.6519	13.0413
	$12.8003 - 0.3370i$		
2	$13.0505 - 0.0090i$	13.041	13.2093
	$13.0693 - 0.0201i$		
3	$13.2183 - 0.0743i$	13.2093	13.3144
	$13.3003 - 0.0901i$		

intervals considered, as listed in Table V and shown in Fig. 5. We list the pole positions corresponding to the two narrowest resonances of each threshold interval. The narrowest of all resonances appear between the opening of the second and third channels (that $N_{\text{open}} = 2$ open channels), respectively, with widths of 9 MeV and 20 MeV. As for the resonances found on the other two intervals, the narrowest of them all has a width of 150 MeV, much larger than the ones found for $N_{\text{open}} = 2$. Note that the second channel is the only one, among the four considered channels, having an orbital angular momentum between the final state mesons. It is possible that the centrifugal barrier between the mesons slows the decay of these tetraquark resonances, according to the mechanism discussed in Ref. [2].

In Table VI, we list the two narrowest resonances between the second and third thresholds, for different m_q in the 0^+ $cc\bar{b}\bar{b}$ system. Depending on the mass of the lightest quark, the width of these resonances can be smaller than 5 MeV or larger than 90 MeV.

Broader resonances can also be found. In Fig. 5 we show a plot of the phase of $\text{Tr}(T)$ for complex energies with real parts between the second and third thresholds and negative

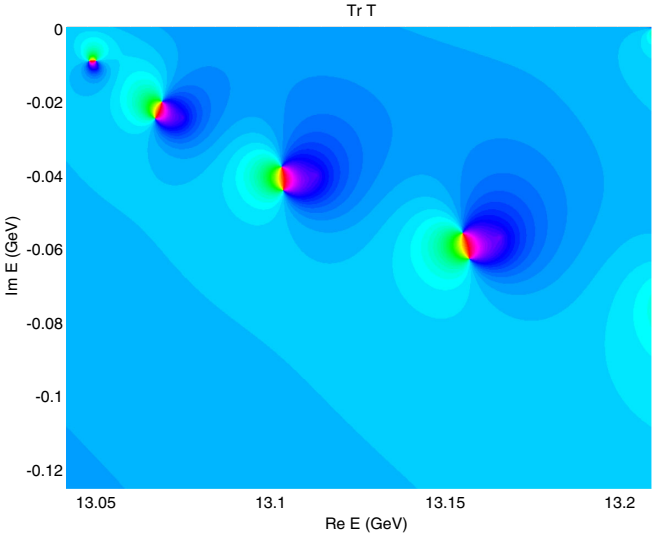

FIG. 5. Plot of $\text{Tr}(T)$, between the second and third thresholds ($N_{\text{open}} = 2$), for the $cc\bar{b}\bar{b}$ system with $L = 0$, $P = +$, and $\xi = +1$. Note the existence of four resonances with $\Gamma/2 < 60$ MeV.

imaginary parts. Four resonances can be observed, all of them with widths smaller than 120 MeV. It is interesting to note the position of the four resonances in the complex plane, approximately forming a straight line.

Doing the same study for $\xi = -1$, we also find several resonances. In Table VII, we compare these resonances and those with $\xi = +1$, for $N_{\text{open}} = 2$ and $m_q = m_c$. Interestingly, in contrast to what happens for the bound states, not only do resonances exist for $\xi = -1$, but they also have similar energies to the ones of the $\xi = +1$ resonances. The real parts of the pole positions are very close, and the imaginary parts are of the same order of magnitude. This result can be understood if we note that what makes the results differ for the two values of ξ is the presence of the nonlocal potential. When we are above the threshold, the wave function becomes oscillatory and the convolution of the wave function with the nonlocal potential in Eq. (43) vanishes if the potential varies slowly. In this way, only the local potential becomes important well above the threshold, and, consequently, the behavior of two resonances becomes similar.

For the $qq\bar{c}\bar{c}$ we are also able to find some resonances. The narrowest of them were between the opening of the second and third channels, similar to what happens on the $qq\bar{b}\bar{b}$ system. A study of these resonances for $N_{\text{open}} = 2$ and varying m_q is presented in Table VIII. We find that the most stable of the two resonances has a width that does not vary much with m_q, having always a value in the range of 35–41 MeV. The width of the second in contrast increases monotonically from 76 MeV to 108 MeV as the mass m_q decreases from 1.3 GeV to 0.4 GeV. Broader resonances also exist here, as we show in Fig. 6.

C. Comparison with other models

We compare our model (C) with two other models for this system, defined in Sec. III D, namely one similar to our triple string flip-flop potential, but without a double Y sector in the potential (B) and the simple colorless flip-flop model (A). The results of these three models are compared in Table IX. When we remove the double Y sector from our

TABLE VI. Resonances in the 0^+ $qq\bar{b}\bar{b}$ system, with $\xi = +1$, with varying quark mass m_q. E_2 and E_3 are the energies of the thresholds of the second and third channels.

m_q[GeV]	E[GeV]	E_2	E_3
1.30	$13.0505 - 0.0090i$	13.041	13.2093
	$13.0693 - 0.0201i$		
1.00	$12.7679 - 0.0011i$	12.5854	12.7686
	$12.5945 - 0.0080i$		
0.70	$12.2054 - 0.0043i$	12.1998	12.4065
	$12.2234 - 0.0256i$		
0.40	$12.0028 - 0.0264i$	11.9836	12.2342
	$12.0471 - 0.0463i$		

TABLE VII. Comparison of pole positions found for $\xi = +1$ and $\xi = -1$ for the 0^+ $cc\bar{b}\bar{b}$ system.

	E[GeV]	
N_{open}	$\xi = +1$	$\xi = -1$
1	$12.7011 - 0.2293i$	$12.7355 - 0.2522i$
	$12.8003 - 0.3370i$	$12.8505 - 0.3733i$
2	$13.0505 - 0.0090i$	$13.0503 - 0.0113i$
	$13.0693 - 0.0201i$	$13.0765 - 0.0268i$
3	$13.2183 - 0.0743i$	$13.2361 - 0.0673i$
	$13.3003 - 0.0901i$	$13.3057 - 0.0822$

TABLE VIII. Resonances for the 0^+ $qq\bar{c}\,\bar{c}$ system, with $\xi = +1$ and varying quark mass m_q.

m_q[GeV]	E[GeV]	E_2	E_3
1.30	$6.5744 - 0.0225i$	6.5530	6.7545
	$6.6226 - 0.0475i$		
1.00	$6.0787 - 0.0250i$	6.0547	6.2675
	$6.1319 - 0.0538i$		
0.70	$5.6450 - 0.0272i$	5.6179	5.8493
	$5.7035 - 0.0639i$		
0.40	$5.3650 - 0.0275i$	5.3373	5.6059
	$5.4351 - 0.0848i$		

model, we still have bound states, for sufficiently small quark masses. For the color independent simple flip-flop model, the binding is even bigger than in our model, even though the double Y sector is not present at all.

Therefore, we see that the presence of a double Y sector in the four-quark potential is not necessary for the existence of bound states with exotic tetraquark quantum numbers. This result has been observed by other authors, namely

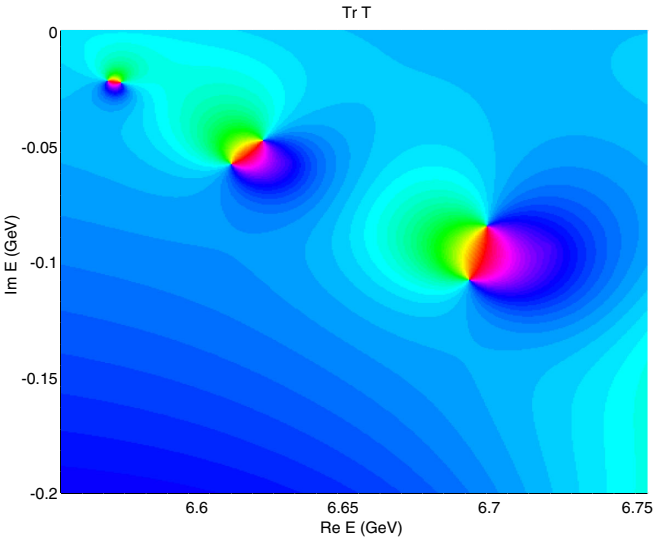

FIG. 6. Plot of $\mathrm{Tr}(T)$, between the second and third thresholds ($N_{\text{open}} = 2$), for the $cc\bar{c}\bar{c}$ system with $L = 0$, $P = +$, and $\xi = +1$. Note the existence of three resonances with $\Gamma/2 < 90$ MeV.

TABLE IX. Binding energies (in MeV) for the 0^+ $qq\bar{b}\bar{b}$ system, $\xi = +1$, with three different models: A—color-independent simple flip-flop; B—color-dependent simple flip-flop; and C—color-dependent triple flip-flop.

m_q[GeV]	A	B	C
1.60	29.5	…	…
1.30	32.3	…	0.4
1.00	36.6	0.3	1.4
0.70	45.8	2.4	4.2
0.40	85.9	17.3	20.3

[71,72,77] where bound states are found for a string flip-flop potential without including any double Y configuration.

All these bound state results are for $s(-1)^{L_r} = +1$ and $\xi = +1$ (see Table I), which correspond to $S_{12} = S_{34} = 0$, and so $J^P = 0^+$ for s, c and b quarks and for light quarks with $I_{12} = 1$. However, for $I_{12} = 0$, exchange symmetry imposes $S_{12} = 1$, which gives quantum numbers 1^+.

VI. DISCUSSION AND CONCLUSION

In this work we briefly review recent experimental and lattice QCD results on tetraquarks, to motivate our approach to unitarize the tetraquark studies. We extend the existing techniques to solve tetraquarks in quark models, fully unitarizing for the first time the triple string flip-flop potential to study bound states and resonances in light-light-antiheavy-antiheavy systems $qq\bar{Q}\bar{Q}$. Consistent with the previous computations with simpler flip-flop potentials, we find several tetraquark bound states and resonances [71,72,77].

Comparing with recent lattice QCD results [15,45,85,86], which found bound states but are not yet able to address resonances, we find a qualitative dynamical agreement in the sense that binding is favored when the light quark q gets lighter and the heavy antiquark $\bar{Q}$ gets heavier.

However, concerning the symmetry and quantum numbers, our results contradict the very recent lattice QCD results in Refs. [15,45,85,86]. In lattice QCD, attraction is only found in scalar isosinglet and vector isotriplet channels, while here we only find bound states (and hence the maximum attraction) for $S_{12} = 0$ and $I = 1$ (scalar isotriplet) or $S_{12} = 1$ and $I = 0$ (vector isosinglet) channels. Also note that the lattice results are consistent with the theoretical predictions of bound $qq\bar{Q}\bar{Q}$ systems with $\bar{Q}$ heavy enough [3–13], which imply the heavy antidiquark $\bar{Q}\bar{Q}$ color wave function is a triplet 3.

Notice we verified that the presence of the double Y sector in the flip-flop potential is not required for our tetraquark bound states. Indeed, we note that the solutions with $\xi = +1$ are mostly color symmetric, while those with $\xi = -1$ are mostly color antisymmetric. This means our bound states are mostly color symmetric, contrary to what one would expect, but consistent with the fact that

removing the double Y sector from the potential does not destroy all the bound states. As for the lattice results, they are indeed color antisymmetric as one would expect. The attractive channels have the same symmetry for spin and isospin as they are either scalar isosinglet ($S_{12}=0$ and $I=0$) or vector isotriplet ($S_{12}=1$ and $I=1$), and so, as the space symmetry is even, the color symmetry has to be negative for the total wave function to be antisymmetric.

Let us analyze the mechanism why we obtain attraction for the color symmetric case and repulsion in the color antisymmetric case. For the $qq\bar{Q}\bar{Q}$ system, if we consider only two channels (related by quark and antiquark exchange), the scattering equation becomes

$$\hat{T}\psi(\mathbf{r})+V^D\psi(\mathbf{r})+\xi\int d^3\mathbf{r}'v(\mathbf{r},\mathbf{r}')\psi(\mathbf{r}') = E\left(\psi(\mathbf{r})+\xi\int d^3\mathbf{r}'\gamma(\mathbf{r},\mathbf{r}')\psi(\mathbf{r}')\right), \quad (86)$$

calculated from Eq. (43). We see that it depends on $V_{I,II}-\frac{V_I+V_{II}}{6}$. When the ground state is $v_0=V_I$, we have $V_{I,II}=\frac{1}{3}V_I$, and so this becomes $\frac{V_I-V_{II}}{6}$. Since V_I is the ground state, we have $V_I<V_{II}$, and therefore

$$\frac{V_I-V_{II}}{6}<0. \quad (87)$$

Since the function Φ in the integrand is nodeless (because it is the ground state),

$$\Phi(\boldsymbol{\rho}_{13},\boldsymbol{\rho}_{24})^*\Phi(\boldsymbol{\rho}_{14},\boldsymbol{\rho}_{23})>0. \quad (88)$$

Therefore, in this limit we have

$$v(\mathbf{r},\mathbf{r}')<0 \quad (89)$$

for $r'\to\infty$ and fixed r. The same result occurs if we exchange r and r'. Then, in Eq. (86) the nonlocal potential will be mostly attractive for $\xi=+1$ and mostly repulsive for $\xi=-1$. This confirms our results.

To summarize, we develop fully unitarized techniques to study tetraquarks with quark models, and to search for bound states and resonances. Asymptotically, the four quark system with a string flip-flop potential reduces to coupled two-body meson-meson systems, with nonlocal potentials that vanish at long distances, thus solving the Van der Waals problem. However, we find that the string flip-flop potential still remains attractive enough to produce $qq\bar{Q}\bar{Q}$ bound states with quantum numbers not observed in recent lattice QCD computations.

It should be noted that different solutions to remove the excessive attraction exist [87,88]. For instance, attraction may change if the nonlocal potentials change signs in the region where $r_1\sim r_2$, and the presence of the $g_{\alpha\beta}$ operator cancels in part the effect of $v_{\alpha\beta}$. We expect that our results will motivate future studies of different solutions to this excessive attraction.

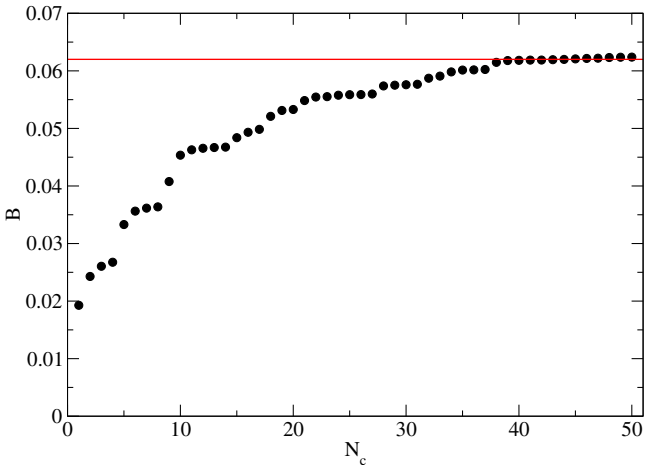

FIG. 7. Binding energy B in natural dimensionless units for the potential $\min(V_{MM},V_{MM'})$ in the case of $\gamma=0$ and $M/m=5$. The dots show the evolution of B as a function of the size N_c of variational basis. As a benchmark, the solid line represents the binding energy computed by Ref. [13].

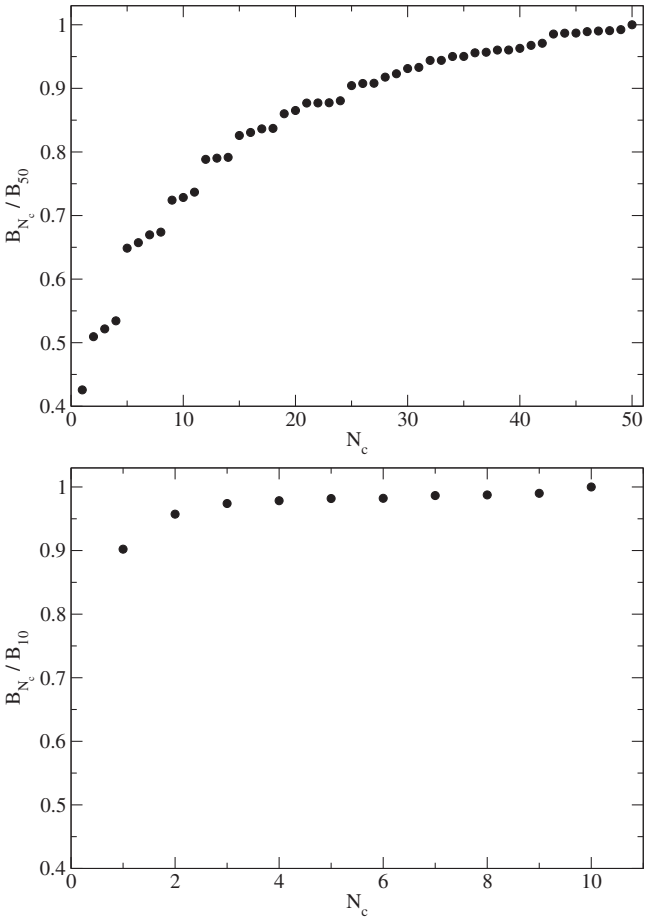

FIG. 8. Evolution of the computed binding energy for the $cc\bar{b}\bar{b}$ system, (top) simple flip-flop potential, (bottom) color-dependent flip-flop.

APPENDIX: VARIATIONAL BASIS BENCHMARK

Using as a benchmark the results in Ref. [13] for the tetraquark binding energy, we test the convergence of our variational basis. Our variational basis is exact in the limit of $N_c \to \infty$, but in practice we have to truncate the basis for a finite number of components N_c, and we want to verify the number of components we are using is correct.

We find that the convergence of our variational basis is slower for the case of the unphysical simple flip-flop potential, but very fast for the color-structure dependent triple flip-flop potential used in this work.

In Fig. 7 we compare the computed binding energy of an exotic system in which $M/m = 5$ and $\sigma = 1$ and compare the result with the one of Refs. [13,88]. To obtain a better binding energy than the one obtained with the variational ansatz of Ref. [13], we need at least 50 channels.

Nevertheless, this is not a problem with our variational basis in general but rather an inadequacy of it applied to the simple flip-flop potential. Indeed, our basis was constructed to obtain the correct asymptotic behavior of any $q_1q_2\bar{q}_3\bar{q}_4$ system. The simple flip-flop potential does not exhibit the correct asymptotic behavior because, since the potential does not depend on color structure, it may produce an asymptotic two-meson state with the incorrect color wave function. Therefore, it is no surprise that the convergence of our basis is so slow for the colorless flip-flop potential.

For our color dependent flip-flop potential, the convergence is much faster. Convergence becomes even faster for a larger M/m quotient. For instance, in the case of $qq\bar{b}\bar{b}$ with $m_q = 0.70$ GeV, the binding energy computed for just one scattering channel is already 96% of the value obtained with $N_c = 10$ (where the convergence is excellent), and with $N_c = 2$ it is 99%.

Comparison of the convergence of the method for the color-dependent flip-flop potential here presented and the simple flip-flop potential is presented in Fig. 8, in the $cc\bar{b}\bar{b}$ system.

[1] R. L. Jaffe, Phys. Rev. D **15**, 267 (1977).
[2] P. Bicudo and M. Cardoso, Phys. Rev. D **83**, 094010 (2011).
[3] J. P. Ader, J. M. Richard, and P. Taxil, Phys. Rev. D **25**, 2370 (1982).
[4] J. l. Ballot and J. M. Richard, Phys. Lett. B **123B**, 449 (1983).
[5] L. Heller and J. A. Tjon, Phys. Rev. D **35**, 969 (1987).
[6] J. Carlson, L. Heller, and J. A. Tjon, Phys. Rev. D **37**, 744 (1988).
[7] H. J. Lipkin, Phys. Lett. B **172**, 242 (1986).
[8] D. M. Brink and F. Stancu, Phys. Rev. D **57**, 6778 (1998).
[9] B. A. Gelman and S. Nussinov, Phys. Lett. B **551**, 296 (2003).
[10] J. Vijande, F. Fernandez, A. Valcarce, and B. Silvestre-Brac, Eur. Phys. J. A **19**, 383 (2004).
[11] D. Janc and M. Rosina, Few-Body Syst. **35**, 175 (2004).
[12] T. D. Cohen and P. M. Hohler, Phys. Rev. D **74**, 094003 (2006).
[13] J. Vijande, A. Valcarce, and J.-M. Richard, Phys. Rev. D **76**, 114013 (2007).
[14] M. Born and R. Oppenheimer, Ann. Phys. (Berlin) **389**, 457 (1927).
[15] P. Bicudo and M. Wagner, Phys. Rev. D **87**, 114511 (2013).
[16] M. Alekseev *et al.* (COMPASS Collaboration), Phys. Rev. Lett. **104**, 241803 (2010).
[17] A. Dzierba, D. Krop, M. Swat, S. Teige, and A. Szczepaniak, Phys. Rev. D **69**, 051901 (2004).
[18] A. R. Dzierba, D. Krop, M. Swat, S. Teige, and A. P. Szczepaniak, Phys. Rev. D **73**, 072001 (2006).
[19] A. Bondar *et al.* (Belle Collaboration), Phys. Rev. Lett. **108**, 122001 (2012).
[20] S. Choi *et al.* (Belle Collaboration), Phys. Rev. Lett. **100**, 142001 (2008).
[21] Z. Q. Liu *et al.* (Belle Collaboration), Phys. Rev. Lett. **110**, 252002 (2013).
[22] K. Chilikin *et al.* (Belle Collaboration), Phys. Rev. D **90**, 112009 (2014).
[23] T. Xiao, S. Dobbs, A. Tomaradze, and K. K. Seth, Phys. Lett. B **727**, 366 (2013).
[24] M. Ablikim *et al.* (BESIII Collaboration), Phys. Rev. Lett. **110**, 252001 (2013).
[25] M. Ablikim *et al.* (BESIII Collaboration), Phys. Rev. Lett. **112**, 132001 (2014).
[26] M. Ablikim *et al.* (BESIII Collaboration), Phys. Rev. Lett. **111**, 242001 (2013).
[27] M. Ablikim *et al.* (BESIII Collaboration), Phys. Rev. Lett. **112**, 022001 (2014).
[28] M. Ablikim *et al.* (BESIII Collaboration), Phys. Rev. Lett. **113**, 212002 (2014).
[29] R. Aaij *et al.* (LHCb Collaboration), Phys. Rev. Lett. **112**, 222002 (2014).
[30] R. Aaij *et al.* (LHCb Collaboration), Phys. Rev. Lett. **115**, 072001 (2015).
[31] M. Cardoso and P. Bicudo, AIP Conf. Proc. **1030**, 352 (2008).
[32] T. Hyodo, Y.-R. Liu, M. Oka, K. Sudoh, and S. Yasui, Phys. Lett. B **721**, 56 (2013).
[33] Y. Jin, S.-Y. Li, Y.-R. Liu, Z.-G. Si, and T. Yao, Phys. Rev. D **89**, 094006 (2014).
[34] Y. Ikeda, B. Charron, S. Aoki, T. Doi, T. Hatsuda, T. Inoue, N. Ishii, K. Murano, H. Nemura, and K. Sasaki, Phys. Lett. B **729**, 85 (2014).

[35] A. L. Guerrieri, M. Papinutto, A. Pilloni, A. D. Polosa, and N. Tantalo, *Proc. Sci.*, LATTICE2014 (2015) 106.
[36] S. Prelovsek, C. Lang, L. Leskovec, and D. Mohler, Phys. Rev. D **91**, 014504 (2015).
[37] L. Leskovec, S. Prelovsek, C. Lang, and D. Mohler, *Proc. Sci.*, LATTICE2014 (2015) 118, http://pos.sissa.it/cgi-bin/reader/contribution.cgi?id=214/118.
[38] M. Lüscher, Commun. Math. Phys. **105**, 153 (1986).
[39] M. Lüscher, Commun. Math. Phys. **104**, 177 (1986).
[40] C. Lang, D. Mohler, S. Prelovsek, and M. Vidmar, Phys. Rev. D **84**, 054503 (2011).
[41] J. J. Dudek, R. G. Edwards, C. E. Thomas, and D. J. Wilson (Hadron Spectrum Collaboration), Phys. Rev. Lett. **113**, 182001 (2014).
[42] M. Wagner (YETM, Collaborations), *Proc. Sci.*, LATTICE2010 (2010) 162.
[43] M. Wagner (ETM Collaboration), Acta Phys. Pol. B Proc. Suppl. **4**, 747 (2011).
[44] Z. S. Brown and K. Orginos, Phys. Rev. D **86**, 114506 (2012).
[45] P. Bicudo, K. Cichy, A. Peters, B. Wagenbach, and M. Wagner, Phys. Rev. D **92**, 014507 (2015).
[46] S. Godfrey and N. Isgur, Phys. Rev. D **32**, 189 (1985).
[47] S. Capstick and N. Isgur, Phys. Rev. D **34**, 2809 (1986).
[48] P. J. A. Bicudo and J. E. Ribeiro, Phys. Rev. D **42**, 1611 (1990).
[49] P. J. A. Bicudo and J. E. Ribeiro, Phys. Rev. D **42**, 1625 (1990).
[50] P. J. A. Bicudo and J. E. Ribeiro, Phys. Rev. D **42**, 1635 (1990).
[51] G. Rupp, S. Coito, and E. van Beveren, Acta Phys. Pol. B Proc. Suppl. **5**, 1007 (2012).
[52] C. Alexandrou and G. Koutsou, Phys. Rev. D **71**, 014504 (2005).
[53] F. Okiharu, H. Suganuma, and T. T. Takahashi, Phys. Rev. D **72**, 014505 (2005).
[54] N. Cardoso, M. Cardoso, and P. Bicudo, Phys. Rev. D **84**, 054508 (2011).
[55] M. Cardoso, N. Cardoso, and P. Bicudo, Phys. Rev. D **86**, 014503 (2012).
[56] N. Cardoso and P. Bicudo, Phys. Rev. D **87**, 034504 (2013).
[57] M. Karliner and H. J. Lipkin, Phys. Lett. B **575**, 249 (2003).
[58] R. Jaffe and F. Wilczek, Eur. Phys. J. C **33**, s38 (2004).
[59] R. Jaffe and F. Wilczek, Phys. World **17**, 25 (2004).
[60] P. Bicudo and G. Marques, Phys. Rev. D **69**, 011503 (2004).
[61] F. J. Llanes-Estrada, E. Oset, and V. Mateu, Phys. Rev. C **69**, 055203 (2004).
[62] Y. Koma and M. Koma, Nucl. Phys. **B769**, 79 (2007).
[63] P. M. Fishbane and M. T. Grisaru, Phys. Lett. B **74**, 98 (1978).
[64] T. Appelquist and W. Fischler, Phys. Lett. B **77**, 405 (1978).
[65] R. Willey, Phys. Rev. D **18**, 270 (1978).
[66] S. Matsuyama and H. Miyazawa, Prog. Theor. Phys. **61**, 942 (1979).
[67] M. B. Gavela, A. Le Yaouanc, L. Oliver, O. Pène, J. C. Raynal, and S. Sood, Phys. Lett. B **82B**, 431 (1979).
[68] G. Feinberg and J. Sucher, Phys. Rev. A **27**, 1958 (1983).
[69] H. Miyazawa, Phys. Rev. D **20**, 2953 (1979).
[70] H. Miyazawa, in *Proceedings, High-energy Nuclear Interactions and Properties of Dense Nuclear Matter, Hakone, 1980*, Vol. 2*, Iii.224–226 (Hayashi-kobo, Tokya, 1980).
[71] M. Oka, Phys. Rev. D **31**, 2274 (1985).
[72] M. Oka and C. Horowitz, Phys. Rev. D **31**, 2773 (1985).
[73] J. Carlson and V. R. Pandharipande, Phys. Rev. D **43**, 1652 (1991).
[74] J. Vijande, A. Valcarce, J.-M. Richard, and N. Barnea, Few-Body Syst. **45**, 99 (2009).
[75] M. Beinker, B. Metsch, and H. Petry, J. Phys. G **22**, 1151 (1996).
[76] S. Zouzou, B. Silvestre-Brac, C. Gignoux, and J. Richard, Z. Phys. C **30**, 457 (1986).
[77] F. Lenz, J. T. Londergan, E. J. Moniz, R. Rosenfelder, M. Stingl, and K. Yazaki, Ann. Phys. (N.Y.) **170**, 65 (1986).
[78] P. Bicudo and M. Cardoso, Phys. Lett. B **674**, 98 (2009).
[79] A. M. Green, C. Michael, and M. E. Sainio, Z. Phys. C **67**, 291 (1995).
[80] A. M. Green, J. Lukkarinen, P. Pennanen, and C. Michael, Phys. Rev. D **53**, 261 (1996).
[81] P. Pennanen, A. M. Green, and C. Michael, Phys. Rev. D **59**, 014504 (1998).
[82] V. G. Bornyakov, P. Yu. Boyko, M. N. Chernodub, and M. I. Polikarpov, arXiv:hep-lat/0508006.
[83] N. Akbar and B. Masud, Eur. Phys. J. A **48**, 25 (2012).
[84] V. I. Lebedev and D. N. Laikov, Dokl. Math. **59**, 477 (1999).
[85] B. Wagenbach, P. Bicudo, and M. Wagner, J. Phys. Conf. Ser. **599**, 012006 (2015).
[86] J. Scheunert, P. Bicudo, A. Uenver, and M. Wagner, Acta Phys. Pol. B Proc. Suppl. **8**, 363 (2015).
[87] G. A. Miller, Phys. Rev. D **37**, 2431 (1988).
[88] J. Vijande, A. Valcarce, and J.-M. Richard, Phys. Rev. D **87**, 034040 (2013).